Precursor-Driven Bcc−Fcc Order−Order Transition of Sphere-Forming Block Copolymer/Homopolymer Blend

Yen-Yu Huang,[†] Jen-Yung Hsu,[†] Hsin-Lung Chen,*[,†] and Takeji Hashimoto*[,‡]

Department of Chemical Engineering, National Tsing Hua University, Hsin-Chu, 30013, Taiwan, and Advanced Science Research Center, Japan Atomic Energy Agency, Naka-gun, Ibaraki Prefecture 319-1195, Japan

Received January 10, 2007; Revised Manuscript Received March 2, 2007

ABSTRACT: We disclose a precursor-driven order−order transition (OOT) between bcc and fcc lattices in a sphere-forming blend of a poly(ethylene oxide)-*block*-poly(1,4-butadiene) (PEO-*b*-PB) and a PB homopolymer (h-PB). The blend as cast from toluene exhibited a metastable trapped fcc (t-fcc) phase, which showed no sign of transformation into bcc phase on heating to 260 °C. Annealing the as-cast blend at −20 °C disturbed the long-range order of t-fcc due to crystallization of PEO within the spherical microdomains. A significant portion of the rather disorderly arranged crystalline domains relaxed to grains having the equilibrium bcc lattice, when the PEO crystals were melted at elevated temperatures. The bcc grains thus developed then acted as the precursor to induce a transformation of t-fcc phase to bcc phase on heating up to 205 °C. Since the t-fcc phase was not completely wiped out through this process, a bcc-to-fcc OOT assisted by the residual t-fcc precursor set in on heating from 205 to 260 °C where fcc became the stable packing symmetry. Subsequent cooling from 260 °C recovered the bcc phase and the blend cooled to 110 °C was essentially fcc free. Because of the absence of fcc grain, the thermodynamically prescribed bcc-to-fcc OOT could no longer take place on reheating. Our results revealed the necessity of bcc or fcc precursor for initiating the relevant OOT and hence implied a high activation barrier associated with the transition. The activation barrier was proposed to be entropic in origin stemming from the deformations of PB blocks and h-PB chains in the lattice transition proceeding through the Bain distortion mechanism.

Introduction

Microphase separation in diblock copolymer (A-*b*-B) and its blend with the corresponding homopolymer (A-*b*-B/h-A) may yield nanoscale microdomains with lamellar, cylindrical or spherical geometry.[1] The spherical domains thus formed have been found to pack almost exclusively in body-centered cubic (bcc) lattice. In addition to bcc packing, closely packed spheres (CPS) in face-centered cubic (fcc) or hexagonal closely packed (hcp) lattices have also been predicted theoretically.[2,3] On basis of the self-consistent mean-field (SCMF) calculation, Matsen and Bates developed a phase diagram for neat A-*b*-B that prescribed a CPS phase situating in a narrow temperature region between bcc and disordered phase.[2] Recently, a CPS phase with fcc packing has been found to coexist with a disordered micelle phase over 4 K temperature interval in a sphere-forming poly(ethylene oxide)-*block*-poly(1,4-butadiene) (PEO-*b*-PB).[4] Fcc phase has also been reported for an elastomeric triblock copolymer, poly(1,3-cyclohexadiene)-*block*-poly(ethylene-*co*-but-1-ene)-*block*-poly(1,3-cyclohexadiene), when the sample was subjected to a flow treatment at 493 K followed by an annealing at 473 K.[5]

In the case of the blends of A-*b*-B with h-A, the phase behavior is governed not only by the segregation strength and the volume fractions of A or B blocks, but also by the volume fraction of h-A in the A domains and the factor $\alpha = M_{h-A}/M_{b,A}$ (with M_{h-A} and $M_{b,A}$ being the molecular weights of h-A and A block, respectively) that determines the extent of solublization of h-A chains into A block chains emanating from the domain interface.[6] The SCMF calculation showed that the composition window of CPS phase in A-*b*-B/h-A blend became broader than that in neat A-*b*-B.[7] In a previous study, we have revealed the presence of fcc-packed PEO spheres in a blend of a symmetric PEO-*b*-PB and a h-PB,[8] where the system was shown to undergo an order−order transition (OOT) from bcc to fcc phase on heating. It is noteworthy that CPS phase has been identified more prevalently among the diblock copolymer solutions with low-molecular-weight selective solvents,[9] in which the interactions between the coronal blocks and the solvent molecules played a role in micelle ordering.

The present study is an extension of our previous work on bcc−fcc OOT of PEO-*b*-PB/h-PB blend. Here we examine the transition process in further detail through systematic SAXS heating and cooling experiments. It will be shown that the OOT is influenced by the thermal history of the sample, and this effect strongly implies a precursor-driven mechanism underlying the transition, where the OOT becomes inaccessible once the system does not contain the bcc or fcc precursor prior to the transition. We shall prove that the previously observed OOT of the PEO-*b*-PB/h-PB blend[8] is due to the precursor-driven OOT to be reported in this paper. This precursor-driven mechanism is phenomenologically similar to the self-nucleation in atomic or molecular crystallization, where the residual nuclei persisted in the melt promotes the crystallization upon cooling. The activation energy barrier associated with the bcc−fcc OOT in the present blend will be discussed in the light of the Bain distortion mechanism found for the bcc−fcc lattice transitions of metal systems[10] and block copolymer micelles formed in low-molecular-weight solvents.[11]

* Authors to whom correspondence should be addressed. E-mail: H.-L.C.) hslchen@mx.nthu.edu.tw; (T.H.) hashimoto.takeji@jaea.go.jp.
[†] Department of Chemical Engineering, National Tsing Hua University.
[‡] Advanced Science Research Center, Japan Atomic Energy Agency.

10.1021/ma070066f CCC: $37.00
Published on Web 04/14/2007

Experimental Section

Materials. The PEO-*b*-PB with the polydispersity index (M_w/M_n) = 1.04 was synthesized by sequential anionic polymerization of butadiene and ethylene oxide (Polymer Source, Inc.). The M_n of PEO block ($M_{b,PEO}$) was 7.5×10^3 and M_n of PB block ($M_{b,PB}$) was 5.5×10^3. This PEO-*b*-PB has a slightly longer PEO block than the sample used in the previous study ($M_{b,PEO} = 6.0 \times 10^3$, $M_{b,PB} = 5.0 \times 10^3$).[8] The 1,4-addition PB homopolymer with $M_n = 2.73 \times 10^3$ was also synthesized by anionic polymerization (Polymer Source, Inc.). The blend with the overall PEO volume fraction (f_{PEO}) of 0.17 was prepared by solvent casting. PEO-*b*-PB and h-PB were first dissolved in toluene at room temperature (ca. 27 °C). The microphase-separated blend was obtained by removing most of the solvent on a hot plate at 80 °C, followed by drying in vacuo at 60 °C for 2 h for complete removal of residual solvent. A portion of the as-cast blend was stored at −20 °C for 8 h prior to the SAXS experiment. This treatment, which allowed the PEO blocks to crystallize in a large portion of the microdomains, is crucial for inducing the formation of bcc phase on heating, as will be demonstrated later.

SAXS Measurement. The thermally induced phase transitions of the blend in the melt state were detected by the temperature-dependent SAXS measurement. The SAXS instrument was equipped with an 18 KW rotating-anode X-ray generator operated at 30 kV × 400 mA (MCA Science Co, Ltd., Yokohama, now Bruker Co, Ltd., M18XHF, Ibaraki Pref., Japan), a 1.5 m camera with a graphite monochromator, and a one-dimensional position-sensitive proportional counter. The Cu Kα line ($\lambda = 0.154$ nm) was used. The intensity profile was output as the plot of the scattering intensity (I) vs the magnitude of the scattering vector, $q = (4\pi/\lambda)\sin(\theta/2)$ (θ = scattering angle). The SAXS profiles were corrected for the absorption, the air scattering, the slit-height and slit-width smearing effect, and then for the background arising from thermal diffuse scattering (TDS). The intensity level of TDS was assumed to be a constant over the q range covered in this study and its magnitude was determined from the slope of Iq^4 vs q^4 plot at the high-q region ($q > 1.3$ nm^{-1}).

Both heating and cooling experiments were conducted in the SAXS measurement. The thermal treatments were operated under N_2 atmosphere in a temperature controlled sample cell.[12] Figure 1 illustrates the thermal protocols adopted for as-cast blend (part a) and −20 °C annealed blend (part b) for the SAXS experiments. For the SAXS measurement at each temperature, the sample was first equilibrated for 30 min followed by data acquisition for another 30 min. Therefore, the sample was kept at each temperature for 60 min. This annealing time was sufficient for resolving the sequence of thermally induced phase transition of interest.

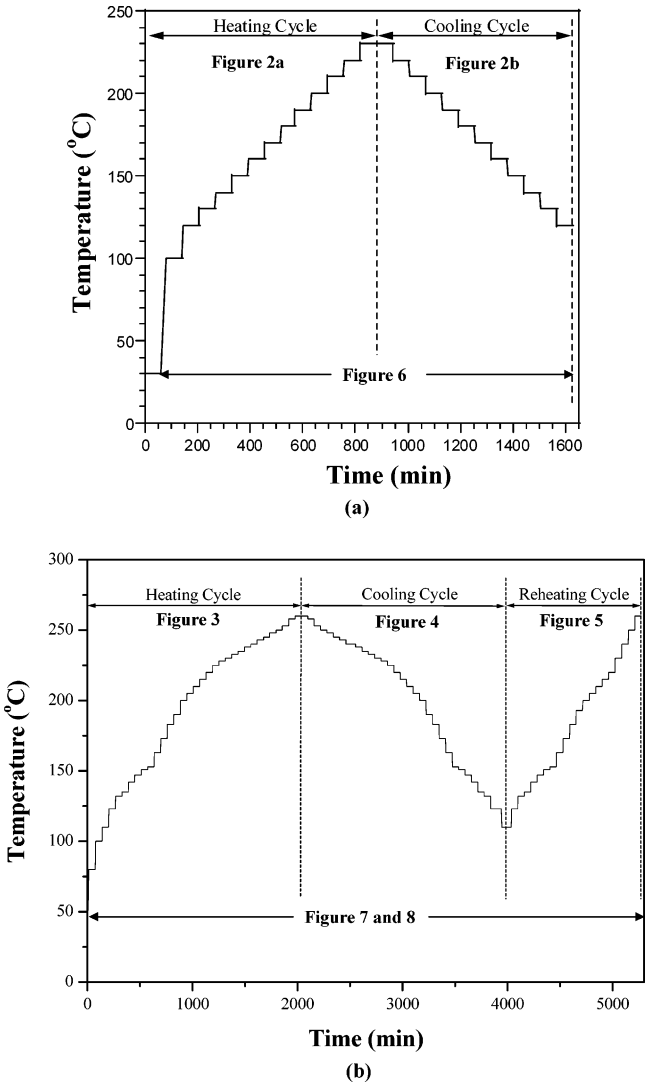

Figure 1. Thermal protocols adopted in the SAXS measurements in the present study. Part a is for the blend directly heated from the as-cast state, while part b is for the blend having been annealed at −20 °C prior to the heating cycle. Three types of thermal treatment, heating, cooling and reheating cycle, were conducted. Their respective time windows are marked by the solid arrows. The figures showing the results obtained from the thermal protocols are also indicated.

Results

SAXS has been widely utilized to distinguish the type of lattice symmetry in diblock copolymers based upon the relative positions of the diffraction peaks. In the case of sphere-forming systems the characteristic peak positions following the ratios of $1:(4/3)^{1/2}:(8/3)^{1/2}:(11/3)^{1/2}:(12/3)^{1/2}$... signal the formation of fcc lattice, while the ratios of $1:2^{1/2}:3^{1/2}:4^{1/2}$... indicate bcc packing.[13] In the present study, the fcc and bcc peaks are marked by the opened and solid arrows in the SAXS profiles, respectively.

Parts a and b of Figure 2 present the SAXS profiles of the as-cast blend collected in situ in the heating and subsequent cooling cycle, respectively. In the plot, we adopt the reduced scattering vector q/q_m in order to clearly distinguish the type of lattice symmetry at each temperature, where q was reduced by q_m with q_m being the primary peak position at each temperature. The temperature dependence of q_m can be separately traced by $D = 2\pi/q_m$ shown later in Figure 6. Interestingly, the as-cast blend contains only fcc phase at 30 °C (i.e., the onset of the heating experiment) as neither $2^{1/2}$ nor $3^{1/2}$ bcc peak is identified in the profile. This fcc phase remains stable throughout the heating to 230 °C without showing any sign of transformation to bcc phase. The subsequent cooling does not induce any structural change either [Figure 2b]. These observations appear to conflict with our previous study showing the occurrence of a bcc-to-fcc OOT on heating.[8] As a matter of fact, the sample used in the previous study had somehow been stored at −20 °C for more than 8 h prior to the SAXS heating experiment. It will be demonstrated below that this thermal treatment is a key for inducing the formation of bcc phase and hence the occurrence of bcc−fcc OOT on heating.

Figure 3 shows the SAXS profiles of the blend collected in a heating cycle from 100 to 260 °C after an annealing at −20 °C for 8 h. The low-temperature annealing allows PEO blocks to crystallize in a large portion of the spherical domains through homogeneous nucleation[14] and such a crystallization disturbs the long-range order of the spheres.[15] The disturbance of lattice packing is evidenced by the broad primary peak in the SAXS profile obtained by heating the crystalline blend to 100 °C [Figure 3a]. In this case, the microdomains cannot relax to attain their original long-range order even after the melting

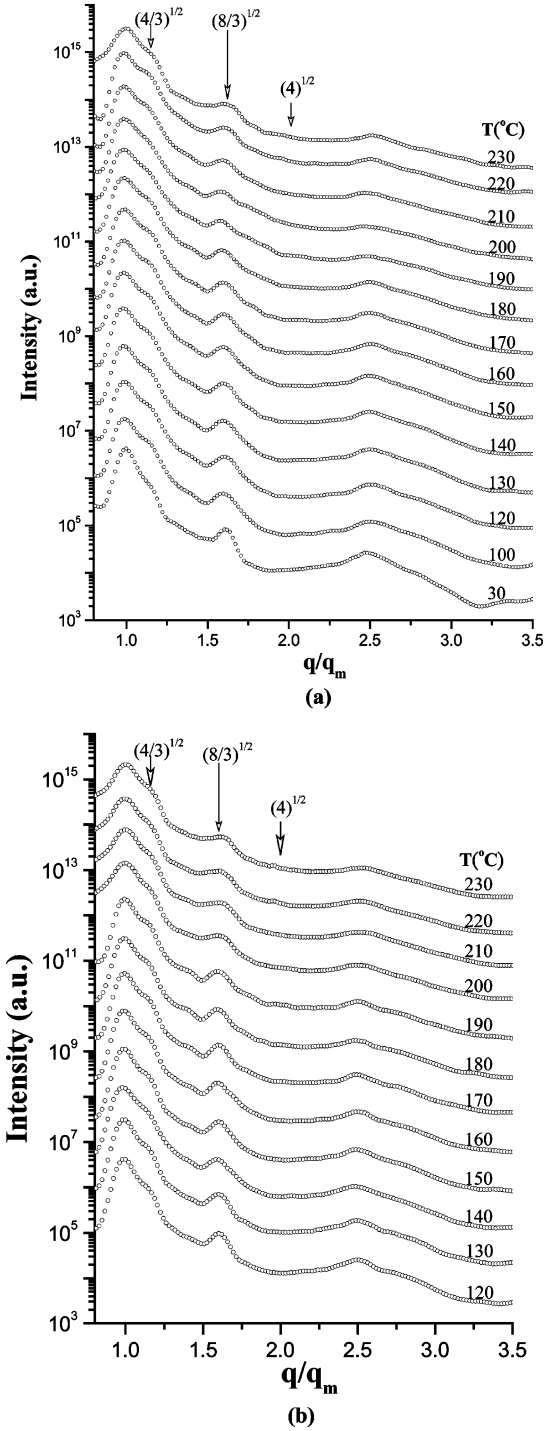

Figure 2. Series of SAXS profiles of the as-cast blend collected in situ at various temperatures from (a) 30 to 230 °C in the heating cycle and (b) subsequent cooling from 230 to 120 °C. The thermal protocol subjected to this blend is shown in Figure 1a. The scattering profiles are presented as a function of q/q_m with q_m being the position of the first-order lattice peak at each temperature. The change in q_m with temperature can be evaluated from that in D ($=2\pi/q_m$) with T shown in Figure 6.

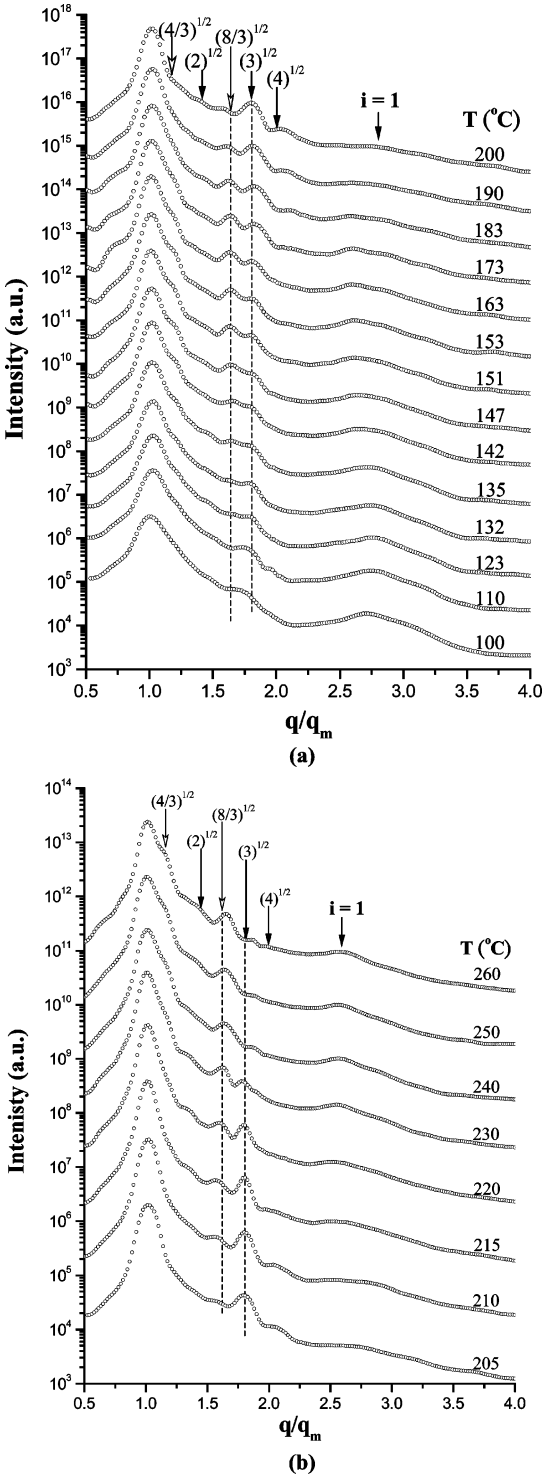

Figure 3. Series of SAXS profiles of the −20 °C annealed blend collected in situ at various temperatures from (a) 100 to 200 and (b) 205 to 260 °C in the heating cycle. The thermal protocol subjected to this blend is shown in Figure 1b. The scattering profiles are presented as a function of q/q_m with q_m being the position of the first-order lattice peak at each temperature. The change in q_m with temperature can be evaluated from that in D ($=2\pi/q_m$) with T shown in Figure 8. The opened arrows identify the characteristic peak positions relative to the first-order peak position ($(4/3)^{1/2}$: $(8/3)^{1/2}$...) that the fcc lattice should exhibit, while the solid arrows pinpoint the relative peak positions ($2^{1/2}$: $3^{1/2}$: $4^{1/2}$...) associated with the bcc phase. The broad peak marked by "$i = 1$" is the first-order peak for form factor of the spherical microdomain.

of PEO crystals. The primary peak sharpens on further heating from 100 to 142 °C, showing the development and growth of the ordered grains. Interestingly, a $3^{1/2}$ diffraction peak associated with bcc lattice now appears clearly at $T \geq 123$ °C together with the fcc peaks. The $3^{1/2}$ peak grows whereas $(4/3)^{1/2}$ and $(8/3)^{1/2}$ fcc peaks diminish progressively with increasing temperature toward 200 °C, showing a transition from fcc to bcc phase. The occurrence of this transition process attests that bcc is indeed the thermodynamic equilibrium packing symmetry below 200 °C. Such an OOT is not accessible by heating the bcc-free as-cast blend due to a high activation energy barrier

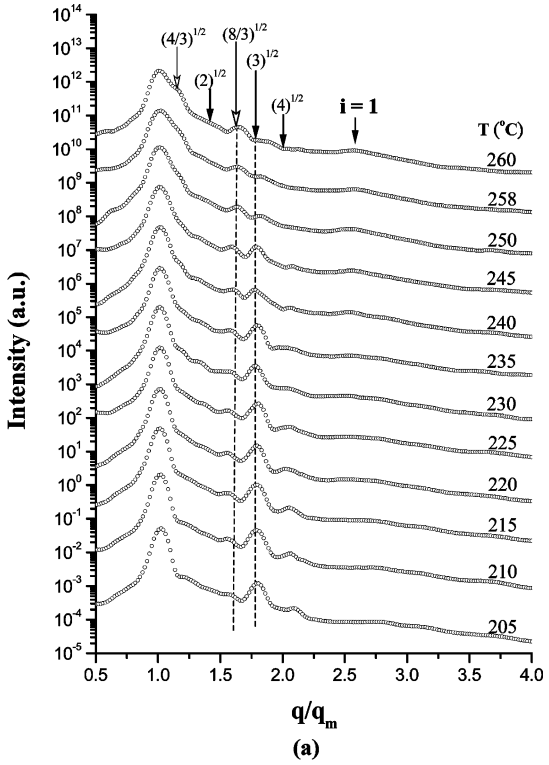

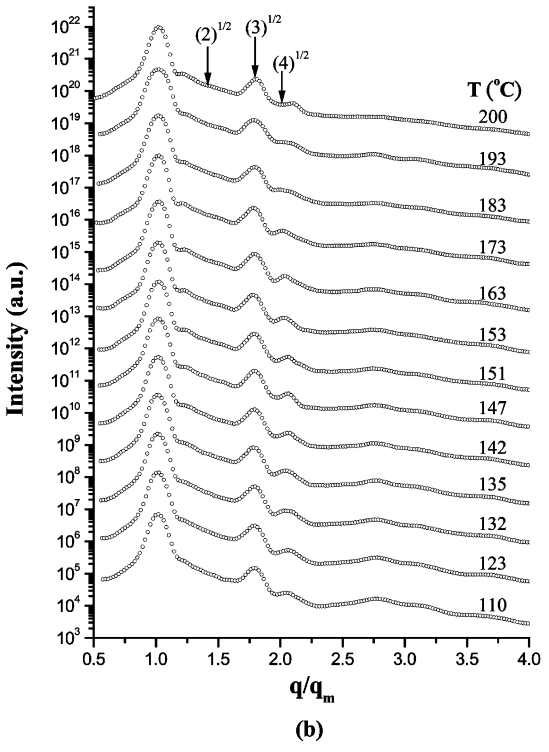

Figure 4. Series of SAXS profiles of the annealed blend collected in situ at various temperatures from (a) 260 to 205 and (b) 200 to 110 °C in the cooling cycle from the fcc phase at 260 °C. The change in q_m with temperature can be evaluated from that in D ($=2\pi/q_m$) with T shown in Figure 8. The data were obtained with the protocol shown in Figure 1b.

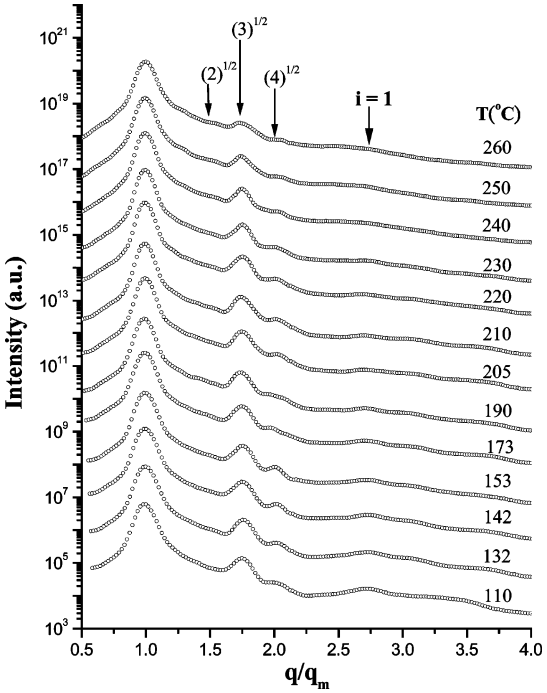

Figure 5. Series of SAXS profiles collected in situ at temperatures from 110 to 260 °C in the reheating cycle from the complete bcc order at 110 °C. The bcc-to-fcc OOT observed in the first heating cycle (*cf.* Figure 3b) no longer occurs up to 260 °C, as bcc phase is found to span the whole temperature window. The change in q_m with temperature can be evaluated from that in D ($=2\pi/q_m$) with T shown in Figure 8.

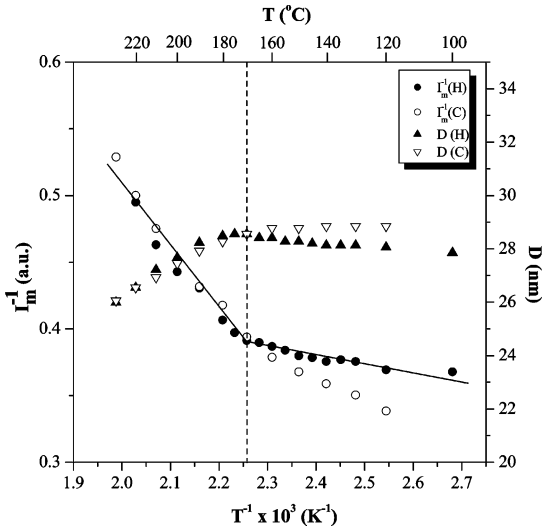

Figure 6. I_m^{-1} and D vs T^{-1} plots for the as-cast PEO-*b*-PB/h-PB blend. The boundary between t-fcc and fcc phases is marked at 170 °C by the vertical dashed line, which is determined by the slop change in I_m^{-1} in the heating cycle. In the cooling cycle, I_m^{-1} and D closely agree with those in the heating cycle when temperature is increased above 170 °C. A large hysterysis stemming from the metastable nature of the trapped fcc phase is found below 170 °C. The parenthesis in the symbol denotes the thermal treatment where H represents the I_m^{-1} collected in the heating cycle and C represents that collected in the cooling cycle. The temperature dependence of D is similar to that in I_m^{-1}.

for OOT. However, if we introduce crystallization into the system, the crystallization driving force is sufficiently large to knock the fcc-packed spheres away from their original positions. When the system is subsequently heated to melt the PEO crystals, a significant portion of the rather disorderly arranged spherical domains relax to pack into the equilibrium bcc lattice. The bcc grains thus formed somehow act as the precursors or nuclei for the growth of bcc phase, such that a fcc-to-bcc OOT becomes accessible with increasing temperature.

Figure 3b presents the SAXS profiles collected by further heating from 205 to 260 °C. Over this temperature range, fcc phase is seen to grow in expense of bcc phase above 210 °C as manifested by the intensification and diminishment of $(8/3)^{1/2}$ and $3^{1/2}$ peak with increasing temperature, respectively. At

230 °C a shoulder corresponding to the $(4/3)^{1/2}$ fcc peak appears beside the primary peak and the $(8/3)^{1/2}$ peak dominates over the neighboring $(3)^{1/2}$ bcc peak. Combining the results of Figure 3a and b, the thermally induced phase transition in the −20 °C annealed blend on heating is found to follow the sequence of mixed bcc/fcc phase, bcc phase, and fcc phase. Now the observed bcc-to-fcc transition (with the onset temperature of the transition being ca. 205 °C) is consistent with the previous finding for another PEO-*b*-PB/h-PB blend having also been annealed at −20 °C prior to the SAXS heating experiment.[8] Nevertheless, the transition in the present system ($M_{b,PEO} = 7.5 \times 10^3$, $M_{b,PB} = 5.5 \times 10^3$) occurs at about 80 °C higher than that of the previously studied system, indicating the stability of bcc phase is enhanced significantly with a minor increase (ca. 25%) of PEO block length. It is noted that a complete bcc or fcc order is never attained under the thermal protocol adopted in the heating cycle, as residual trace of fcc or bcc phase is found to coexist with the dominant counterpart even at 200 (*cf.* Figure 3a) or 260 °C (*cf.* Figure 3b), respectively.

A SAXS cooling experiment was conducted from the state of predominant fcc phase at 260 °C after the series of the heating experiment described above for the −20 °C annealed blend to test the thermal reversibility of the bcc−fcc OOT. Figure 4 presents the temperature-dependent scattering patterns collected in the cooling cycle. It can be seen that bcc phase grows progressively in the expense of fcc phase between 250 and 205 °C. The temperature-dependent SAXS profiles clearly show an OOT from fcc to bcc phase in the cooling process, thereby demonstrating that bcc−fcc OO*T* is thermally reversible.

The SAXS cooling profiles at temperatures lower than 210 °C are shown in Figure 4b. It can be seen that the fcc phase originally existed below 200 °C in the heating cycle [cf. Figure 3a] is no longer present as the bcc phase remains stable all the way down to 110 °C at which the system possesses nearly complete bcc order. This verifies that the fcc phase observed in the heating process below 200 °C in Figure 3a is metastable, and its formation should be associated with the solvent casting process, where the fcc structure seemingly formed first during the solvent evaporation process was somehow trapped into the bulk after complete solvent removal. This metastable fcc phase is called "trapped fcc phase" (t-fcc) here and its formation mechanism will be illustrated in the Discussion.

A reheating experiment was conducted after the blend has been subjected to the heating and cooling cycles (cf. the thermal protocol in Figure 1b). Figure 5 shows the SAXS profiles collected in situ in the reheating cycle. At the onset of the reheating process (i.e., 110 °C) the system exhibits nearly complete bcc order. Interestingly, the bcc-to-fcc OOT observed in the first heating cycle no longer occurs up to 260 °C, as bcc phase is found to span the whole temperature window. This is reminiscent of the result in Figure 2a showing that heating the as-cast blend with complete fcc order does not induce fcc-to-bcc transition. The results hence indicate that the OOT is accessible only if the system contains the bcc/fcc precursor. The fcc precursor is created by the solvent casting which leads to the formation of the metastable t-fcc phase, whereas the bcc precursor is generated by allowing the PEO domains in the as-cast blend to crystallize followed by heating above the melting point of PEO.

Figure 6 displays the temperature dependences of the inverse of the intensity of the primary scattering peak (I_m^{-1}) and the characteristic distance ($D = 2\pi/q_m$) for the as-cast blend. The data were obtained from Figure 2. In this plot, the vertical dashed line represents the approximate onset (170 °C) of the transition

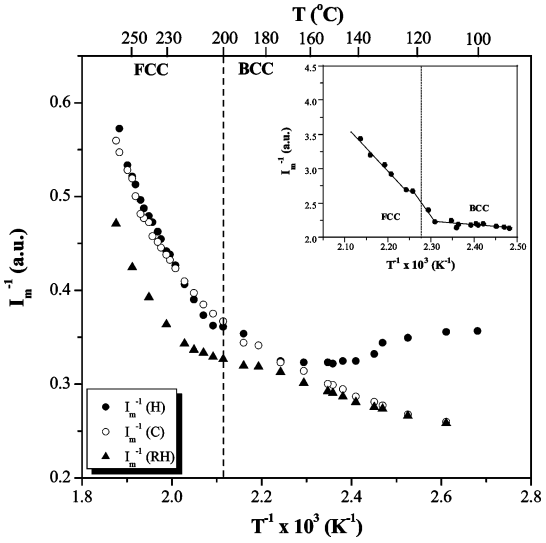

Figure 7. I_m^{-1} vs T^{-1} plots for the −20 °C annealed PEO-*b*-PB/h-PB blend. The boundary between bcc and fcc phases is marked at 200 °C by the vertical dashed line, in that this temperature roughly represents the point where fcc phase vanishes in the cooling cycle. Little hysterysis effect is found across the bcc−fcc OOT at high-temperature (i.e., in the temperature region from 170 to 260 °C), while strong hysterysis stemming from the metastable nature of the trapped fcc phase is found below 170 °C. Through comparing I_m^{-1}s in cooling and reheating cycles, another strong hysterysis is found to appear with reheating the cooled blend. The hysterysis originates from the coexistence of bcc and fcc phase in the onset of cooling. The parenthesis in the symbol denotes the thermal treatment where H represents the I_m^{-1} collected in the heating cycle, C represents that collected in the cooling cycle and RH represents that collected in the reheating cycle. The inset in the figure shows I_m^{-1} vs T^{-1} across the bcc−fcc OOT for the system with shorter PEO block ($M_{b,PEO} = 6.0 \times 10^3$).[8]

boundary between t-fcc and fcc phase upon heating, in which t-fcc phase is a lattice packing that situates in a metastable state generated during solvent removal. The boundary between t-fcc and fcc phase is determined by the slope change of I_m^{-1} in heating run. The temperature dependence of I_m^{-1} in the cooling cycle is characterized by a smooth curve with the I_m^{-1} values closely agreeing with those observed in the heating cycle at $T > 170$ °C. A hysterysis is identified at $T < 170$ °C, where the intensities at a given temperature in the heating and cooling cycles do not agree. Such a hysterysis effect is an indicative of the metastable nature of the t-fcc phase observed below 170 °C. Similar conclusion can also be drawn from the D vs T^{-1}plot.

Figure 7 plots I_m^{-1} against the inverse of absolute temperature for heating, cooling and reheating cycles for the −20 °C annealed blend which exhibits bcc−fcc OOT in the heating and cooling cycles. The vertical dash line represents the approximate onset (200 °C) of the bcc−fcc transition under the temperature protocol used in our study. Little hysterysis effect is found in the temperature range from 170 to 260 °C across the bcc−fcc OOT, where I_m^{-1} associated with the heating run closely agrees with that in the cooling cycle. This means that the corresponding bcc and fcc phases are thermodynamically stable structures and the dynamics of the phase transition is rapid. On the contrary, strong hysterysis stemming from the metastable nature of the t-fcc phase is found below 170 °C, where I_m in the heating cycle (due to bcc/t-fcc structure) is clearly lower than that in the cooling cycle where the corresponding structure is bcc.

I_m in the reheating cycle closely agrees with that in the cooling cycle at $T < 170$ °C, whereas a deviation is found at $T > 170$ °C. The deviation is due to the fact that the system subjected to the cooling experiment contains both bcc and fcc phases at

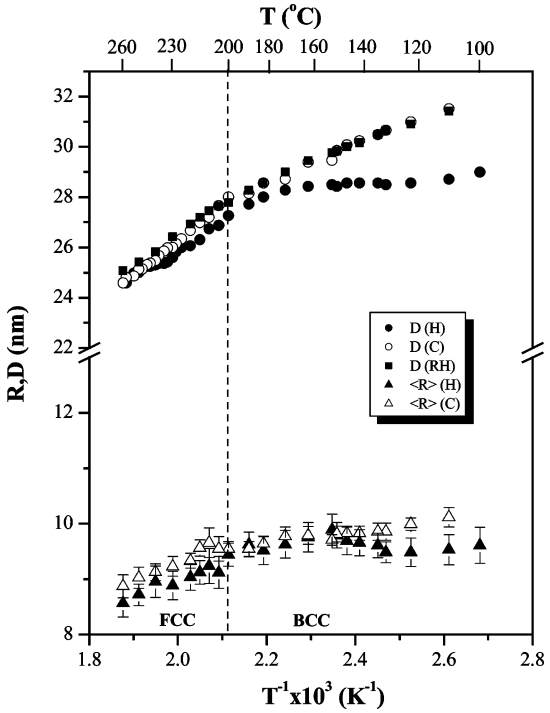

Figure 8. *D* and *R* vs T^{-1} plots for the −20 °C annealed PEO-*b*-PB/h-PB blend. *R* is obtained by fitting the form factor profiles using a polydisperse spherical form factor. The temperature dependences of *D* and *R* display a strong hysterysis below 170 °C due to the presence of trapped fcc phase in the as-cast blend. In the reheating cycle, a very small hysterysis originating from the coexistence of fcc and bcc phase in the onset of cooling cycle is found to appear above 170 °C.

$T > 170$ °C, while the blend is essentially fcc-free in the reheating experiment. Note that vertical dash line for the approximate onset of OOT is irrelevant for I_m^{-1} vs T^{-1} for the reheating run.

Figure 7 also demonstrates that the onset of the bcc−fcc transition is characterized by the change of the slope of the plot. In the previous study, a rather vague discontinuity in I_m^{-1} vs T^{-1} across the bcc−fcc OOT in the system with a shorter PEO block length was suggested with less intensity data points, as shown in the inset of Figure 7.[8] As a matter of fact, a close comparison between the plot of the present system and that shown in the inset indicates that the temperature dependences of I_m^{-1} of both systems across the OOT are essentially identical except for the temperature shift for the OOT. Since more intensity data points are collected over the transition region for the present system, the I_m^{-1} vs T^{-1} plot across the OOT observed should be more accurately characterized by a slope change instead of an abrupt discontinuity. The discontinuity is not observed here because the lattice transformation is not sharp, where bcc and fcc phases coexist over a wide temperature range under the thermal protocol adopted.

Figure 8 dispalys the temperature dependences of D and the average radius *R* of the PEO spherical microdomains for the −20 °C annealed blend. *R* was obtained by fitting the form factor profile shown in Figure 3−5 (with the broad first-order peak marked by "$i = 1$" near $q/q_m \sim 2.75$) using form factor for polydisperse spheres. Similar to I_m, a strong hysterysis is found below 170 °C due to the presence of t-fcc phase in the as-cast blend (*cf.* heating and cooling cycle).

Discussion

The following summarizes the salient features of the bcc/fcc phase and the relevant OOT in the sphere-forming PEO-*b*-PB/h-PB blend derived from the present study:

1. A metastable t-fcc phase develops during solvent casting and the as-cast blend is essentially bcc-free. Heating the as-cast blend does not induce transformation of t-fcc phase to bcc phase in the temperature range where bcc is supposed to be the equilibrium structure.

2. Annealing the as-cast blend at −20 °C allows PEO blocks to crystallize in the microdomains. The crystallization driving force is sufficiently large to knock the fcc-packed spheres away from their original positions, and a significant portion of the rather disorderly arranged domains relax to pack into the equilibrium bcc lattice upon subsequent heating to melt the PEO crystals.

3. The bcc grains thus developed act as the precursors or nuclei to initiate the transformation from t-fcc to bcc phase on heating in the temperature window where the later is the stable structure. The t-fcc phase is however not completely wiped out before reaching the temperature where fcc becomes the favorable packing symmetry. The residual t-fcc grains then serve as the precursors for initiating a bcc-to-fcc transition upon further heating.

4. The conversion from bcc to fcc phase is incomplete on reaching the maximum experimental temperature (260 °C) as some bcc residue still remains to act as the precursor to initiate a reverse fcc-to-bcc OOT in the subsequent cooling cycle. The conversion to bcc order is complete upon cooling to 110 °C at which the system is essentially fcc free.

5. Because of the lack of fcc precursor, reheating the cooled blend can no longer induce the bcc-to-fcc OOT.

Now let us first discuss the origin of t-fcc phase. It is known that block copolymer mesophase in the as-cast state may be nonequilibrium because the solution mesophase of the A-*b*-B/solvent mixture above the threshold polymer concentration for microphase separation may deviate from the equilibrium melt structure of A-*b*-B and such a structure may be trapped into the bulk upon solvent removal, yielding metastable bulk structure in the as-cast sample.[16−18] Although toluene has a slightly closer solubility parameter δ toward PB,[19] it can still be considered as a nearly neutral solvent for PEO and PB because toluene can swell nearly equally well PEO and PB domains. During the solvent evaporation, the increase of the block copolymer concentration tends to increase the effective segregation strength between PEO and PB in the medium of a neutral solvent of toluene, in that the effective interaction parameter, χ_{eff}, can be formulated as $\chi\phi_P$ with ϕ_P being the polymer concentration according to the dilution approximation.[1c,20] Consequently, we expect a series of transitions such as follows to occur with increasing concentration: homogeneous solution → disordered micelles → fcc phase → bcc phase. The fcc phase precedes the bcc lattice, because according to the thermally induced phase transition, fcc phase is favored at smaller χ (or at higher temperature), i.e., $\chi_{bcc} > \chi_{fcc}$. Once the fcc−bcc transition is quite slow compared to the rate of solvent removal, fcc phase will be trapped into the bulk before the completion of the transition, thereby leading to the absence of the expected bcc phase in the as-cast sample (Figure 2a).

The more interesting observation here is the precursor-driven mechanism of the bcc−fcc OOT. bcc-to-fcc transition is accessible when the system contains residual t-fcc grains before reaching the temperature where fcc phase is the stable structure on heating. The converse is true for the t-fcc-to-bcc (on heating) and fcc-to-bcc (on cooling) transitions, where bcc precursor is required to induce the phase transformations. This kind of precursor effect is phenomenologically reminiscent of the self-nucleation encountered in atomic or molecular crystallization;

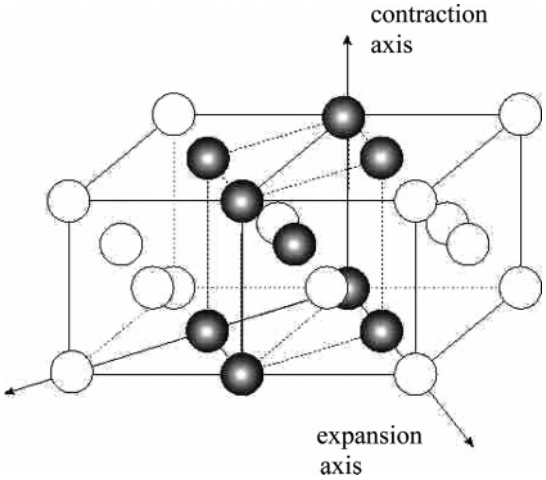

Figure 9. Schematic illustration of one set of Bain distortion for the transition from fcc to bcc lattice, which involves the transformation of a distorted bcc unit cell embedded in two fcc unit cells to a bcc unit cell by compressing along one (100) direction and expanding along two (110) directions of the fcc unit cells.

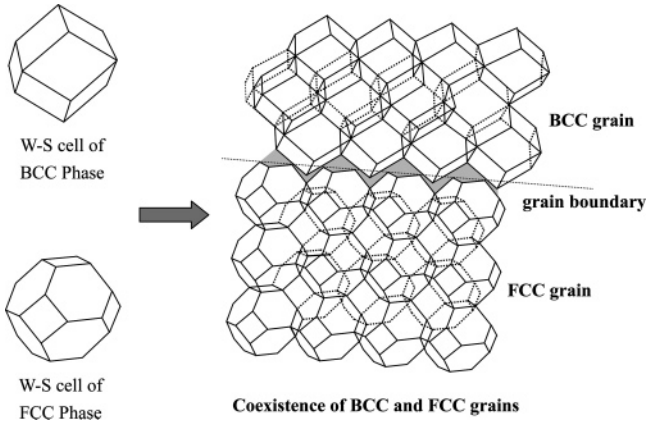

Figure 10. Left: Wigner−Seitz (W−S) cells of the spherical micelles in bcc and fcc lattice. The W−S cell is a truncated octahedron and a dodecahedron for bcc and fcc phase, respectively. Right: In the system containing both bcc and fcc grains, the two types of W−S cells cannot geometrically match with each other at the grain boundaries, such that vacancies are created near the boundaries (i.e., the shaded region).

therefore, bcc−fcc OOT must likewise involve an activation energy barrier which is lowered by the presence of the precursor.

To reveal the nature of the activation energy barrier, we need evoke a plausible pathway through which the OOT takes place. For the crystals formed by metals, bcc−fcc lattice transformation proceeds through the well-known Bain distortion.[10] Such a mechanism was found to be operative in the thermally induced bcc−fcc OOT of the spherical micelles formed by block copolymers in low-molecular-weight selective solvents.[11] For the transition from fcc to bcc phase, the Bain distortion mechanism involves the transformation of a distorted bcc unit cell embedded in neighboring two fcc unit cells to a bcc unit cell by compressing along one (100) direction and expanding along two (110) directions of the fcc unit cells, as illustrated schematically in Figure 9. The contraction may also occur along (010) or (001) direction with the corresponding expansions along (101) and (1*h*01), or (110) and (1*h*10) directions, respectively.[11]

The deformation of unit cells via Bain distortion mechanism is relatively easy for lattices composing of the spherical micelles dispersed in a low-molecular-weight solvent. In the case of A-*b*-B/h-B blend, however, such a lattice distortion will cause the stretching and compression of the coronal blocks and homopolymer chains in the matrix phase; consequently, an activation energy barrier with entropic origin exists for the bcc−fcc transition. Such an activation energy barrier is difficult to be overcome purely by the thermal fluctuation-induced collective motion of the spherical domains to create the unit cell distortion. As a result, the t-fcc phase developed in the as-cast PEO-*b*-PB/h-PB blend is superheated to the temperatures where bcc is supposed to be the stable structure. When the as-cast blend is annealed at −20 °C to perturb the fcc order by PEO crystallization followed by heating to melt the PEO crystals, a portion of the domains would relax to the equilibrium bcc lattice, leading to the coexistence of bcc and t-fcc phase. It is known that the Wigner-Seitz (W−S) cell of the spherical micelles with bcc and fcc packing is a truncated octahedron and a dodecahedron, respectively, as shown in Figure 10.[21,22] In the system containing both bcc and fcc lattices, the two types of W−S cells cannot match with each other geometrically at the grain boundaries, such that vacancies are created near the boundaries (i.e., the shaded region in Figure 10). To eliminate the density dips, the PB coronal blocks or h-PB chains located near the grain boundaries must hence be stretched out of the W−S cells to fill into the vacancies, thereby giving rise to an excess interfacial free energy associated with the conformational entropy loss. In this case, the grain boundaries may be unstable, such that the more stable bcc grains grow from the boundaries in the expense of the t-fcc phase to reduce the interfacial free energy by the local rearrangement of the spherical micelles.

Conclusions

We have revealed a precursor-driven mechanism underlying the OOT between bcc and fcc phase in a sphere-forming PEO-*b*-PB/h-PB blend. The OOT was inaccessible if the system did not contain bcc or fcc precursor prior to the transition. The lack of fcc precursor may be one of the reasons for the prevalent absence of bcc−fcc OOT among the sphere-forming diblock copolymer systems. The activation energy barrier of the OOT was proposed to stem from the stretching and compression of the coronal blocks and homopolymer chains in the matrix phase as the lattice transition occurred through the Bain distortion mechanism. Such an entropic barrier was difficult to be overcome by the thermal fluctuation-induced collective motion of the spherical domains, thereby making the OOT inaccessible in the melt composing of only one type of lattice. Nevertheless, if the bcc or fcc precursor could somehow be generated out of the fcc or bcc matrix, respectively, the bcc/fcc grain boundaries may be unstable due to the geometric mistmatch between the Wigner-Seitz cells of the two types of lattices. Such an interfacial instability will then drive the growth of the stable lattice from the precursor grains. We found that crystallization of PEO blocks at low temperature followed by heating to melt the crystals was an effective approach to induce the development of the precursor with the equilibrium lattice. In this case, the crystallization driving force was sufficiently large to knock the spherical domains away from their original positions and a significant portion of the rather disorderly arranged domains would relax to the equilibrium lattice upon the melting of PEO crystals. Other perturbations such as the application of shear flow may also be useful for inducing the formation of the precursor out of the metastable phase for initiating the growth of the stable lattice structure.

Acknowledgment. We gratefully acknowledge financial support from the National Science Council Taiwan under Contract NSC 94 2216-E-007-002.

References and Notes

(1) (a) Leibler, L. *Macromolecules* **1980**, *13*, 1602. (b) Hashimoto, T.; Shibayama, M.; Fujimura, M.; Kawai, H. In *Block Copolymers-Science and Technology*; Meier, D. J., Ed.; Harward Academic Publishers: London, 1983. (c) Hamley, I. W. *The Physics of Block Copolymers*, Oxford University Press: New York, 1998.

(2) Matsen, M. W.; Bates, F. S. *Macromolecules* **1996**, *29*, 1091.

(3) Semenov, A. N. *Macromolecules* **1989**, *22*, 2849.

(4) Huang, Y.-Y.; Hsu, J.-Y.; Chen, H.-L.; Hashimoto, T. *Macromolecules* **2007**, *40*, 406.

(5) Imaizumi, K.; Ono, T.; Kota, T.; Okamoto, S.; Sakurai, S. *J. Appl. Crystallogr.* **2003**, *36*, 976.

(6) (a) Hashimoto, T.; Tanaka, H.; Hasegawa, H. *Macromolecules* **1990**, *23*, 4378. (b) Tanaka, H.; Hasegawa, H.; Hashimoto, T. *Macromolecules* **1991**, *24*, 240.

(7) (a) Matsen, M. W. *Macromolecules* **1995**, *28*, 5765. (b) Matsen, M. W. *Phys. Rev. Lett.* **1995**, *74*, 4225.

(8) Huang, Y.-Y.; Chen, H.-L.; Hashimoto, T. *Macromolecules* **2003**, *36*, 764.

(9) (a) Hamley, I. W.; Daniel, C.; Mingvanish, W.; Mai, S.-M.; Booth, C.; Messe, L.; Ryan, A. J. *Langmuir* **2000**, *16*, 2508. (b) Bang, J.; Lodge, T. P.; Wang, X.; Brinker, K. L.; Burghardt, W. R. *Phys. Rev. Lett.* **2002**, *89*, 215505. (c) McConnell, G. A.; Gast, A. P.; Huang, J. S.; Smith, S. D. *Phys. Rev. Lett.* **1993**, *71*, 2102. (d) Pople, J. A.; Hamley, I. W.; Fairclough, J. P. A.; Ryan, A. J.; Komanschek, B. U.; Gleeson, A. J.; Yu, G.-E.; Booth, C. *Macromolecules* **1997**, *30*, 5721. (e) Hanley, K. J.; Lodge, T. P.; Huang, C.-I. *Macromolecules* **2000**, *33*, 5918. (f) Lodge, T. P.; Bang, J.; Park, M. J.; Char, K. *Phys. Rev. Lett.* **2004**, *92*, 145501.

(10) (a) Nishiyama, Z. *Martensitic Transformation*; Academic Press: New York, 1978. (b) Olsen, G. H.; Jesser, W. A. *Acta Metall.* **1971**, *19*, 1009. (c) Olsen, G. H.; Jesser, W. A. *Acta Metall.* **1971**, *19*, 1299.

(11) Bang, J.; Lodge, T. P. *J. Phys. Chem. B* **2003**, *107*, 12071.

(12) Hashimoto, T.; Kowsaka, K.; Shibayama, M.; Suehiro, S. *Macromolecules* **1986**, *19*, 750.

(13) Cullity, B. D.; Stock, S. R. *Elements of X-ray Diffraction*; Prentice Hall: Upper Saddle River, NJ, 2001; Chapter 10.

(14) (a) Chen, H.-L.; Hsiao, S.-C.; Lin, T.-L.; Yamauchi, K.; Hasegawa, H.; Hashimoto, T. *Macromolecules* **2001**, *34*, 671. (b) Chen, H.-L.; Wu, J.-C.; Lin, T.-L.; Lin, J. S. *Macromolecules* **2001**, *34*, 6936.

(15) (a) Chen, H.-L.; Li, H.-C.; Huang, Y.-Y.; Chiu, F.-C. *Macromolecules* **2002**, *35*, 2417. (b) Huang, Y.-Y.; Yang, C.-H.; Chen, H.-L.; Chiu, F.-C.; Lin, T.-L.; Liou, W. *Macromolecules* **2004**, *37*, 486.

(16) (a) Hashimoto, T.; Fujimura, M.; Kawai, H. *Macromolecules* **1980**, *13*, 1660. (b) Shibayama, M.; Hashimoto, T.; Kawai, H. *Macromolecules* **1983**, *16*, 1434. (c) Mori, K.; Hasegawa, H.; Hashimoto, T. *Polymer* **1990**, *31*, 2368.

(17) Sakurai, S.; Umeda, H.; Taie, K.; Nomura, S. *J. Chem. Phys.* **1996**, *105*, 8902.

(18) Funaki, Y.; Kumano, K.; Nakao, T.; Jinnai, H.; Yoshida, H.; Kimishima, K.; Tsutsumi, K.; Hirokawa, Y.; Hashimoto, T. *Polymer* **1999**, *40*, 7147.

(19) Brandrup, J.; Immergut, E. H. *Polymer Handbook*; 2nd ed.; John Wiley & Sons Inc.: New York, 1975; Part IV.

(20) The dilution approximation treats concentrated solutions as uniformly swollen melt phases and the phase behavior maps onto those of melts by replacing χ by $\chi\phi_P$. This mean-field approximation is good enough for our qualitative interpretation on the increase of segregation strength with increase of block copolymer concentration during solvent removal.

(21) The Wigner−Seitz (W−S) cell may be constructed according to the following four steps. First, select any lattice site as the origin. Second, start at the origin followed by drawing lines to all its neighboring lattice point. Third, draw the perpendicular bisecting plane of each of these lines. Finally, the space enclosed by the resulting polyhedron is the W−S cell. For block copolymers the W-S cell represents the space occupied by a single micelle in a lattice. It is a rhombic dodecahedron for FCC lattice and a truncated octahedron for BCC phase.

(22) Wigner, E.; Seitz, F. *Phys. Rev.* **1933**, *43*, 804.

MA070066F